

BEAM DYNAMICS DESIGN OF DEBUNCHER SYSTEM FOR J-PARC LINAC ENERGY UPGRADE

M. Ikegami*, KEK, Tsukuba, Japan
 T. Ohkawa, Mitsubishi Heavy Industries Ltd., Kobe, Japan
 T. Morishita, H. Sako, JAEA, Tokai, Japan

Abstract

We will have an energy upgrade for J-PARC linac, where the output beam energy is increased from 181 MeV to 400 MeV. In the energy upgrade, we also plan to replace the debuncher system between the linac and the succeeding ring. The beam dynamics design for the new debuncher system has been performed assuming an advantageous configuration called “the separate-function configuration”.

INTRODUCTION

J-PARC (Japan Proton Accelerator Research Complex) is a high-intensity proton accelerator facility which consists of an injector linac, 3-GeV RCS (Rapid Cycling Synchrotron), and 50-GeV MR (Main Ring) [1]. While the output beam energy of J-PARC linac is currently 181 MeV, we have planned an upgrade of the linac output energy to 400 MeV to ease the space-charge effects in the RCS injection process. Recently, the energy upgrade has been approved by the government for its construction. The upgrade will be realized by adding ACS (Annular Coupled Structure linac) section after existing SDTL (Separate-type Drift Tube Linac) section [2]. At the same time, we also plan to replace the debuncher system installed in the beam transport line between the linac and RCS.

In this paper, the beam dynamics design of the new debuncher system is presented with some simulation results.

BASIC CONCEPT

The debuncher system has the following two roles. One is to reduce the momentum centroid jitter, and the other is to control the momentum spread at the RCS injection. The requirement from the RCS injection is to reduce the sum of the momentum spread and momentum centroid jitter below $\pm 0.2\%$ in full width. This requirement comes from an elaborated injection scheme called “the momentum offset injection” assumed at RCS [4]. We here set the design goal of the debuncher system to $\pm 0.05\%$ each for the momentum spread and momentum centroid jitter with a margin of factor two.

Provided that it is in the linear regime and zero-current limit, the momentum spread and momentum centroid jitter can be simultaneously minimized with a proper choice of debuncher parameters. However, such a double-optimum setting does not exist with finite space-charge effects [3, 5]. In addition, a beam is often subject to a large phase error

and large phase spread in a debuncher system. Then, the momentum spread is prone to be increased by filamentation due to the nonlinearity of the RF forces. Accordingly, we need to properly care about these effects in designing a debuncher system for a high intensity linac.

In the course of the design of the present 181-MeV debuncher system, we devised an advantageous configuration for a two-cavity debuncher system [3]. We refer to it as “the separate-function configuration”. In this configuration, the momentum jitter is corrected with the first debuncher alone, and the momentum spread is separately controlled with the second debuncher. This feature significantly simplifies the tuning procedure for the debuncher system. This separate-function nature is brought about by keeping the beam arrival phase at the second debuncher to -90 deg regardless of the momentum centroid jitter at the linac exit. This is realized by appropriately choosing three debuncher parameters, namely, the drift length between the linac exit and the first debuncher l_1 , that between the first and second debunchers l_2 , and the focal length of the first debuncher f_1 . We should note here that the focal length of the second debuncher f_2 is secured as the tuning knob for the momentum spread control. As the phase error at the second debuncher is minimized with this configuration, it is also advantageous in reducing the filamentation at the second debuncher. In other words, we can build a robust debuncher system against the momentum centroid jitter by adopting this configuration. More detailed discussions on the separate-function debuncher configuration will be found in the reference [3].

In the debuncher system for the energy upgrade, we also plan to adopt the separate-function debuncher configura-

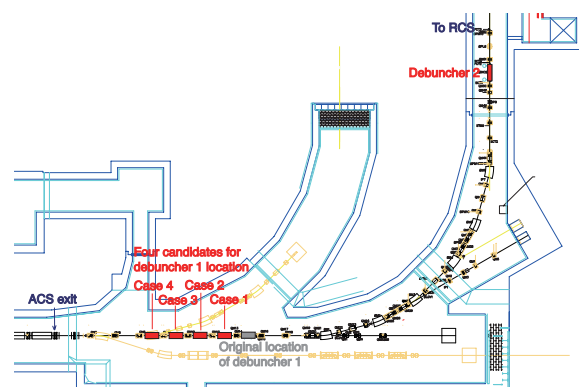


Figure 1: Schematic layout of the debuncher system.

* masanori.ikegami@kek.jp

tion. Figure 1 shows the layout of the debuncher system. The first debuncher is to be installed at the straight section after the linac, and the second debuncher after a 90-degree achromatic arc section.

As for the RF structure for the debuncher cavities, we plan to adopt the ACS with the frequency of 972 MHz. The frequency is the same as the nominal accelerating modules in the ACS section. A debuncher module consists of two ACS tanks connected with a bridge coupler, and each ACS tank has five to six accelerating cells. The RF power is fed through the bridge coupler from a klystron. This configuration is the same as the nominal ACS modules except for the smaller number of accelerating cells in a tank [2]. The debuncher module has a larger bore radius to reduce the beam loss. The bore radius for the first and the second debunchers are to be 35 mm and 42.5 mm, respectively.

DESIGN OPTIMIZATION

There originally was a preliminary design of the 400-MeV debuncher system, and the present magnet layout for the beam transport line was determined assuming the original layout [6]. While it was a two-cavity debuncher system, the separate-function configuration was not assumed in the debuncher design.

In this paper, we review the debuncher design adopting the separate-function debuncher configuration. The optimization of debuncher layout has been performed assuming the existing magnet layout. The location of the first debuncher and the voltages of two debunchers are optimized here. We don't have a flexibility for the second debuncher location to be compatible with the downstream transverse collimator system. In other words, $l_1 + l_2$ is fixed in the present consideration.

To realize the separate-function nature, we need to satisfy the following relation,

$$f_1 = \frac{l_1 l_2}{l_1 + l_2}. \quad (1)$$

In the separate-function configuration, shorter distance for l_1 is preferable to have efficient momentum jitter correction. On the other hand, smaller l_1 results in a higher voltage for the first debuncher cavity from Eq. (1). It requires a larger number of accelerating cells in a tank and hence a longer tank length. As the available space for the debuncher cavity is limited with the present magnet layout, there should be an optimum choice for the first debuncher location. Around the assumed location for the first debuncher, the magnet has a doublet lattice with the period length of 3.7 m. Then, we here consider four locations for the first debuncher with the interval of 3.7 m. Table 1 summarizes the main parameters for the four cases, where V_1 and N_1 respectively denote the required voltage and the number of accelerating cells for the first debuncher. In finding the adequate debuncher voltage, we assume the synchronous phase of -90 deg for the first debuncher. The considered four locations for the first debuncher are also

Table 1: Main parameters for considered four cases

	Case 1	Case 2	Case 3	Case 4
l_1 (m)	22.7	19.0	15.3	11.6
l_2 (m)	68.5	72.2	75.9	79.6
l_1/l_2	0.33	0.26	0.20	0.15
f_1 (m)	17.0	15.0	12.7	10.1
V_1 (MV)	2.84	3.21	3.79	4.77
N_1	9	10	12	15

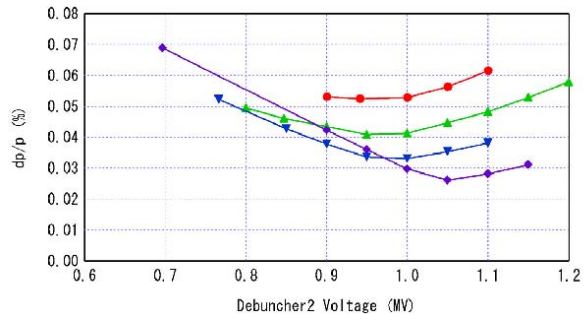


Figure 2: Simulated 99.9 % momentum spread at the RCS injection vs. the voltage of the second debuncher. Red: Case 1, green: Case 2, blue: Case 3, and purple: Case 4.

shown in Fig. 1. Just for reference, l_1 and l_2 for the previous design were 26.4 m and 64.8 m, respectively.

As the momentum spread is subject to space-charge effects and filamentation, it is required to perform particle simulations to find an adequate voltage for the second debuncher. Figure 2 shows PARMILA simulation results for the above four cases. As seen in this figure, the optimum voltage for the second debuncher is only weakly dependent on f_1 and around 1 MV for all four cases. It is also seen that the case with shorter l_1 is advantageous in having smaller momentum spread at the RCS injection.

Figure 3 shows the longitudinal phase space distribution at the RCS injection for the above four cases. In this figure, the simulation results with the energy shift ΔE at the linac exit is also shown. The assumed ΔE is about 0.16 % in the momentum deviation. As the momentum jitter currently experienced with the 181-MeV operation is significantly smaller than ± 0.1 %, the assumed ΔE has a sufficient margin. In Case 1 to 4, the introduced energy shifts are respectively reduced to 30 %, 24 %, 18 %, and 13 % at the RCS injection. As readily seen in Fig. 3, the filamentation is insensitive to the momentum variation in all four cases. It indicates that the nonlinearity at the debunchers are successfully suppressed by adopting the separate-function configuration.

According to the above considerations, Case 4 is the most advantageous in reducing both momentum jitter and momentum spread. It is however difficult to realize Case 4 with the present magnet layout, because the available space can accommodate only 12 accelerating cells or 6 accelerating cells per tank. While the momentum spread in Case 3

Table 2: Main specifications for debuncher cavities

	Cavity #1	Cavity #2
Structure	ACS	ACS
Frequency (MHz)	972	972
Bore radius (mm)	35	42.5
Num. of tanks	2	2
Num. of cells per tank	6	5
Max. E_0 (MV/m)	4.12	4.12
Operation voltage (MV)	3.79	0.98
Max. voltage (MV)	3.84	3.20
Synchronous phase (deg)	-90	-90

is a little larger than that in Case 4, but sufficiently smaller than the design goal of $\pm 0.05\%$. In addition, the energy jitter correction efficiency of 18% is sufficient also considering the jitter currently experienced in the 181-MeV operation. Consequently, we conclude that we adopt Case 3 for the 400-MeV debuncher system.

The main specifications for the debuncher cavities are summarized in Table 2. As seen in this table, the first debuncher voltage only has a slight margin. However, the required voltage for the first debuncher is clearly determined by the debuncher layout. Then, we have concluded that the slim margin is sufficient for the first debuncher. On the other hand, the required voltage for the second debuncher has a larger uncertainty because it depends on the longitudinal emittance and the shape of the longitudinal distribution. Therefore, we have a larger margin for the second debuncher voltage.

The margin for the second debuncher can also be utilized in the future longitudinal painting injection into RCS by introducing a patterned control of the voltage and the synchronous phase during a macro-pulse. In the longitudinal painting, $V_2 \cos \Phi_s$ is supposed to be varied to provide momentum variation keeping $V_2 \sin \Phi_s$ constant. With the separate-function configuration, the momentum variation can be provided by simply varying the second debuncher parameters without sacrificing the momentum jitter correction and momentum spread control. As it is also a significant advantage for the separate-function configuration, we plan to pursue the feasibility of the longitudinal painting in a future study.

SUMMARY

The beam dynamics design of the debuncher system has been performed for the J-PARC linac energy upgrade. The design has been performed assuming the current magnet layout for the beam transport line. In the design, the separate-function configuration is adopted to simplify the tuning procedure and ease the momentum spread due to filamentation. According to PARMILA simulations, the design goals for the momentum spread and the momentum centroid jitter correction are expected to be achieved with a sufficient margin.

Beam Dynamics and Electromagnetic Fields

D01 - Beam Optics - Lattices, Correction Schemes, Transport

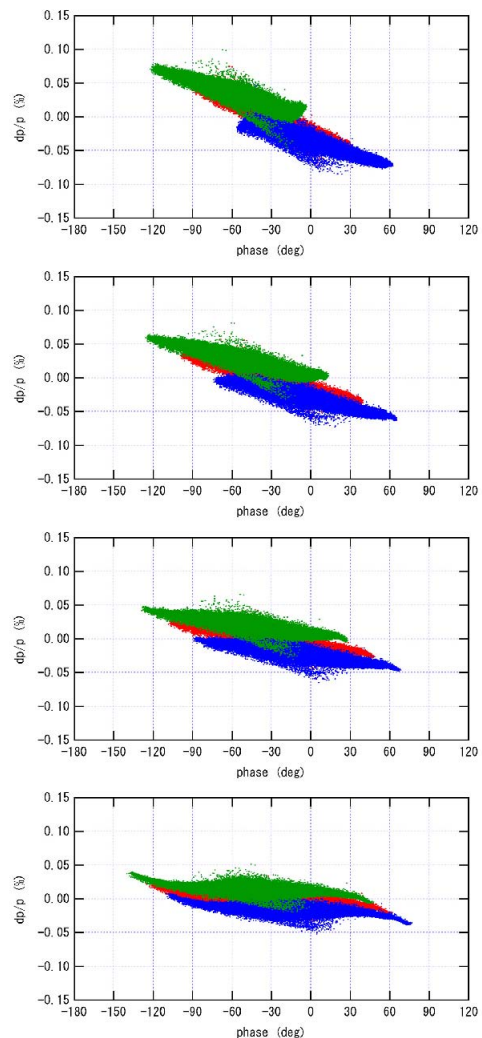


Figure 3: Simulated longitudinal phase space distribution at the RCS injection for four cases, namely, top: Case 1, middle top: Case 2, middle bottom: Case 3, and bottom: Case 4. Results for the following three cases are superimposed; red: $\Delta E = 0$ MeV, green: $\Delta E = -0.775$ MeV, and blue: $\Delta E = 0.825$ MeV.

REFERENCES

- [1] Y. Yamazaki, "Status of J-PARC", in these proceedings.
- [2] H. Ao, et. al., "Improvement in the ACS Cavity Design for the J-PARC Linac Energy Upgrade", LINAC'08, Victoria, September 2008, THP056 (2008).
- [3] T. Ohkawa, M. Ikegami, Nucl. Instrum. Meth. A 581 (2007) 606.
- [4] M. Yamamoto et. al., "Longitudinal Beam Dynamics on 3 GeV PS in JAERI-KEK Joint Project", EPAC'02, Paris, June 2002, p. 1073 (2002).
- [5] T. Ohkawa, M. Ikegami, Nucl. Instrum. Meth. A 576 (2007) 274.
- [6] M. Matsuoka, et. al., "Design of Beam Transport Line between Linac and 3-GeV Synchrotron for the JAERI-KEK joint project", Procs of the 27th Linear Accelerator Meeting in Japan, Kyoto 2002, p. 243 (in Japanese).